J. Ocean Univ. China (Oceanic and Coastal Sea Research)
DOI 10.1007/s11802-017-3221-z
ISSN 1672-5182, 2017 16 (5): 738-746
http://www.ouc.edu.cn/xbywb/
E-mail:xbywb@ouc.edu.cn

Numerical Modeling of Local Scour Around Hydraulic Structure in Sandy Beds by Dynamic Mesh Method

FAN Fei[1), 2)], LIANG Bingchen[2), *], BAI Yuchuan[1)], ZHU Zhixia[3)], and ZHU Yanjun[3)]

1) *State Key Laboratory of Hydraulic Engineering Simulation and Safety*, *Tianjin University*, *Tianjin* 300000, *P. R. China*
2) *Shandong Province Key Laboratory of Ocean Engineering*, *Ocean University of China*, *Qingdao* 266100, *P. R. China*
3) *Jiangsu Province Water Transport Engineering Technology Research Center*, *Nanjing* 21000, *P. R. China*

(Received June 8, 2016; revised June 3, 2017; accepted June 25, 2017)

Abstract Local scour, a non-negligible factor in hydraulic engineering, endangers the safety of hydraulic structures. In this work, a numerical model for simulating local scour was constructed, based on the open source code computational fluid dynamics model OpenFOAM. We consider both the bedload and suspended load sediment transport in the scour model and adopt the dynamic mesh method to simulate the evolution of the bed elevation. We use the finite area method to project data between the three-dimensional flow model and the two-dimensional (2D) scour model. We also improved the 2D sand slide method and added it to the scour model to correct the bed bathymetry when the bed slope angle exceeds the angle of repose. Moreover, to validate our scour model, we conducted and compared the results of three experiments with those of the developed model. The validation results show that our developed model can reliably simulate local scour.

Key words local scour; sandy bed; dynamic mesh; sand slide

1 Introduction

Local scour around hydraulic structures is a complicated problem that has confounded engineers for many years. After much effort, the numerical model for local scour has vastly improved and a number of scour model software programs have been constructed, such as Flow3D and CCHE3D, which are now being applied in many fields. Bombar *et al*. (2013) used CCHE3D to investigate local scour around piers under non-uniform sediment conditions. Vasquez and Walsh (2009) utilized Flow3D to study the local scour around complex piers subject to tidal flow. These authors contributed to the current improved scour modeling ability. However, there remain a number of limitations. For instance, Flow3D adopts the finite difference method to discretize Navier-Stokes equations, which affects accuracy of modeled result when the shape of the object is complex despite the adoption of the Fractional-Area-Volume-Obstacle-Representation (FAVOR) method in FLOW3D. CCHE3D uses the finite element method to discretize the governing equations, which results in a high computational overhead.

To compensate for the above shortcomings, a number of local scour models have been constructed based on the finite volume method. Huang *et al*. (2009) added the bedload transport model into the ANSYS Fluent model to study the scour hole profile around bridge piers. This model uses an adaptive mesh σ coordinate system that can easily fit object shapes. Based on OpenFOAM, Liu (2008) constructed the solver FOAMSCOUR to study wave-induced the local scour around piers. In Liu's model, the parameters of sediment transport are mapped from a 3D to a 2D mesh to solve the Exner equation, which affects accuracy during the mapping process. To maintain precision in scour analyses around wind farm foundations, Stahlmanm (2013) solved the Exner equation using the finite area method (FAM). Jacobsen (2011) studied the evolution of sand beaches and analyzed the impact of interpolation methods on the conservation of mass. This author has since constructed a new 2D sand slide model for unstructured mesh (Jacobsen, 2015). Other researchers have also constructed local sediment transport models based on their own computational fluid dynamics (CFD) models with respect to beach evolution and other issues (Roulund *et al*., 2005; Zhao *et al*., 2015; Baykal, 2014; Furhman *et al*., 2014; Sumer *et al*., 2011; Petersen, 2014).

Although many local scour models have been constructed, none of their codes are open access. In this work, we constructed a local scour model based on the open source code CFD model OpenFOAM version OpenFOAM-extend-3.1 for an upcoming scour study. We developed and introduced bedload and suspended load sediment trans-

* Corresponding author. Tel: 0086-532-66781129
E-mail: bingchen@ouc.edu.cn

port models into the OpenFOAM source code. In the scour model, bed shear stress is calculated based on the Reynolds stress rather than by the traditional method, whereby we assume that the velocity in the vertical direction fits the parabolic distribution, and the Eulerian volume-of-fluid (VOF) method was used to capture the free surface of the fluid, and the dynamic mesh method was adopted to capture the bed surface. A 2D sand slide model was built to correct the bed level when bed slope exceeds the angle of repose. Finally, we conducted three test cases to test and validate the sand slide model, suspended transport model and scour model, respectively. The results confirm that the modeling results agree well with the measured data overall. The scour model is reliable in reasonably simulating the scour development process.

2 Theory Description

2.1 Flow Model and Turbulence Model

2.1.1 Flow model equation

The governing equations of fluid flow are the incompressible continuity equation and the Reynolds-averaged Navier-Stokes equation (Jacobsen, 2011), as follows, respectively:

$$\nabla\cdot\boldsymbol{U}=0\,, \tag{1}$$

$$\frac{\partial\rho\boldsymbol{U}}{\partial t}+\nabla\cdot\rho\boldsymbol{U}\boldsymbol{U}^{\mathrm{T}}=-\nabla p+\rho g+\nabla\cdot\left[\mu\nabla\boldsymbol{U}+\rho\tau\right]+\sigma_T\kappa_\gamma\nabla\gamma\,, \tag{2}$$

where, U is the velocity field in Cartesian coordinates; ρ is the multiphase flow density; p is the total pressure; g is the gravitational acceleration; μ is the dynamic molecular viscosity; τ is the Reynolds stress tensor; $\kappa\gamma$ is the curvature of the interface; σ_T is the surface tension constant; γ is the volume fraction of fluid.

2.1.2 Turbulence model

We chose the conventional k-ε turbulence closure model to calculate the parameters related to the turbulence of fluid flow (Stahlmanm, 2013), as follows:

$$\frac{\partial(\rho k)}{\partial t}+\frac{\partial}{\partial x_i}(\rho\cdot k\cdot u_i)=\frac{\partial}{\partial x_j}\left[(\mu+\frac{\mu_t}{\sigma_j})\frac{\partial k}{\partial x_j}\right]+P_k+P_b-\rho\varepsilon-Y_M+S_k\,, \tag{3}$$

$$\frac{\partial}{\partial t}(\rho\varepsilon)+\frac{\partial}{\partial x_i}(\rho\varepsilon u_i)=\frac{\partial}{\partial x_j}\left[\left(\mu+\frac{\mu_t}{\sigma_\varepsilon}\right)\frac{\partial\varepsilon}{\partial x_j}\right]+C_{1\varepsilon}\frac{\varepsilon}{k}\left(P_k+C_{3\varepsilon}P_b\right)-C_{2\varepsilon}\rho\frac{\varepsilon^2}{k}+S_\varepsilon\,, \tag{4}$$

$$k=\frac{1}{2}\overline{u_i'u_i'}\,, \tag{5}$$

$$\varepsilon=\nu\overline{\frac{\partial u_i'}{\partial x_k}\frac{\partial u_i'}{\partial x_k}}\,, \tag{6}$$

$$\mu_T=C_\mu\rho\frac{k^2}{\varepsilon}\,, \tag{7}$$

$$\tau_{ij}=\frac{\mu_T}{\rho}\left(\frac{\partial u_i}{\partial x_j}+\frac{\partial u_j}{\partial x_i}\right)-\frac{2}{3}\rho k\sigma_{ij}\,, \tag{8}$$

where, ρ is density of two phase flow, a_w is the volume rate of water, ρ_w is the density of water, ρ_a is the density of air, k is the turbulence kinetic energy, ε is the dissipation rate of turbulence, $c_{1\varepsilon}$=1.44, $c_{2\varepsilon}$=1.99, σ_K=1.0, σ_ε=1.3 , μ_t is turbulence viscosity.

2.2 Sediment Transport Model

Scour is mainly caused by bed erosion induced by the non-equilibrium of the sediment transport flux. The sediment transport flux consists of the bedload and suspended load, which we developed and introduced in this study to the OpenFOAM source code.

2.2.1 Bedload model

Many bedload sediment transport models are available for simulating scour, such as those by Engelund and Meyer-Peter *et al.* (Liu, 2008). In this study, we used the bed load transport model by Huai *et al.* (2011), which describes bedload transport in terms of the Shields and critical Shields numbers, as follows:

$$q_0=11.6(\theta-\theta_c)[\theta^{1/2}-\theta_c^{1/2}]\sqrt{Rgd}\,d,\ \theta\geq\theta_c\,, \tag{9}$$

$$q_0=0,\ \theta<\theta_c\,, \tag{10}$$

$$\theta=\frac{\tau_b}{\rho_{\mathrm{w}}gRd}\,, \tag{11}$$

where, q_0 is the bed load transport rate per unit width in $\mathrm{m^2\,s^{-1}}$; θ is shields number, which can be calculated using Eq. (11); g is gravitational acceleration; d is median grain diameter; R is the relative density of sediment; θ_c is critical shields number.

The critical Shields number is usually given for a flat bed. Allen and Roulund developed a formula (Eq. (12)), in which the effects of the local bed slope on the critical Shields number is taken into account (Jacobsen, 2011; Huai *et al.*, 2011). In addition, the effect of the angle between local bed slope and the local shear stress are considered, which yields a more reasonable computational result. Fig.1 shows the Roulund's formula scheme, in which G_s is the projection of gravity acceleration onto the bed surface.

$$\theta_{cr}=\theta_{c0}(\cos\beta\sqrt{1-\frac{\sin^2\phi\tan^2\beta}{{\mu_s}^2}}-\frac{\cos\phi\sin\beta}{\mu_s})\,, \tag{12}$$

where, θ_{c0} is the critical shields number for a flat bed; ϕ is the angle between bed steepest slope and bed shear stress direction; β is the angle between bed and horizontal plane; μ_s is static friction coefficient.

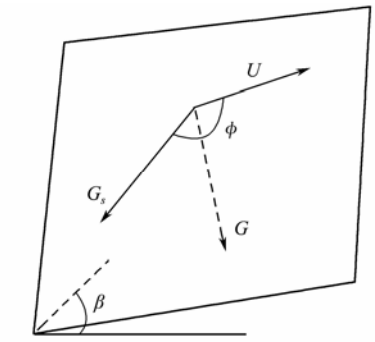

Fig.1 Bed slope effect on critical Shields number.

2.2.2 Suspended load model

The governing equation of the suspended load model is the convection-diffusion equation, which can be expressed as follows:

$$\frac{\partial c}{\partial t}+\nabla\cdot(U-w_s)c=\nabla\cdot(\nu_t\nabla c)\,, \tag{13}$$

where, c is the sediment concentration; U is the flow velocity field; w_s is sediment fall velocity in still water; v_t is diffusivity of sediment, in present work, it equals to turbulence eddy viscosity.

To solve the convection-diffusion equation, we must specify the boundary condition. For the inlet boundary condition, we set the suspended concentration to be zero in the clear water case and at a fixed value if the concentration has been measured. For the outlet boundary, we adopt the Nuemann boundary condition. For the bottom boundary, we set the suspended concentration at a reference height, which is recognized as the boundary of the bed load and specified the suspended load as the bottom boundary condition (Van Rijn, 1987). We can determine the sediment concentration at this reference height as shown below:

$$c_b=0.015\cdot\rho_s\frac{d_{50}T^{1.5}}{\Delta_b D_*^{0.3}}\,, \tag{14}$$

where, c_b is the sediment concentrate at reference level; ρ_s is the density of sand; Δ_b is the distance from reference level to bed; T is the non-dimensional excess shear stress, which we can determine using Eq. (15), as follows:

$$T=\frac{\mu_{sc}\cdot\tau_{sc}-\tau_{cr}}{\tau_{cr}}\,, \tag{15}$$

where, μ_{sc} is the efficiency factor current; τ_{sc} is the bed shear stress caused by current; τ_{cr} is the critical bed shear stress.

2.3 Bed Morphology Model

We can obtain the change in the bed elevation by solving the following Exner equation:

$$\frac{\partial\eta}{\partial t}=\frac{1}{1-n}(-\nabla q_b+D-E)\,, \tag{16}$$

where, η is the bed elevation; n is the porosity of sand; q_b is the bed load transport rate; D is the deposition rate; E is the erosion rate.

We can calculate the total bed load transport rate by Eq. (9), which is scalar, whereas the bed load transport rate in Eq. (16) is vector. We can perform the conversion from scalar to vector using Eq. (17) (Liu, 2008):

$$q_{bi}=q_0\frac{\tau_i}{|\tau|}-C|q_0|\frac{\partial\eta}{\partial x_i},\ i=1,2\,, \tag{17}$$

where, q_{bi} is the bed load transport rate component in the i direction; τ_i is the bed shear stress component in the i direction; C is a constant, with 1.5; i is the horizontal coordinate component, representing the x, y directions, respectively.

$$D=C_c\cdot w_s\,, \tag{18}$$

where C_c is the sediment concentration at the center near the bed and w_s is the sand settling velocity.

There are several empirical models available for calculating the entrainment rate, and in this work, we use the Smith's model (Liu, 2008; Niemann *et al.*, 2011). In this model, γ_0 in Eq. (20) is a constant at 0.0024.

$$E=w_s\cdot\tilde{E}\,, \tag{19}$$

$$\tilde{E}=\frac{0.65\gamma_0(\frac{\theta}{\theta_c}-1)}{1+\gamma_0(\frac{\theta}{\theta_c}-1)}\,. \tag{20}$$

2.4 Dynamic Mesh Model

As mentioned above, the dynamic mesh method is generally applied to obtain the change in the bed elevation. When this change in bed elevation is solved using Eq. (16), the Laplacian equation is then used to compute the displacement of the inner nodes of the mesh (Jasak and Tuković, 2007):

$$\nabla\cdot(\gamma\nabla\nu)=0\,, \tag{21}$$

where v is the displacement field of the mesh points; and γ is the diffusion coefficient, which is used to control the mesh motion. In this study, we chose the inverse distance diffusion coefficient, which is more suitable for simulating scour.

2.5 Sand Slide Model

Once the maximum scour slope angle exceeds the angle of repose, the scour will become unstable, and will yield unreasonable computational results. As such, a sand slide model is needed to smooth the bed surface. Many one-dimensional sand slide models have been developed (Roulund *et al.*, 2005; Niemann *et al.*, 2011), but these are too difficult to apply in 2D problems. Jacobsen (2011) developed a new 2D sand slide model for studying the evolution of sand beaches. In this work, we construct a 2D sand slide model to smooth the bed slope using the

method developed by Jacobsen. Fig.2 shows the face cell of a bed, which must be corrected. To conserve the mass of the sediment, the location of the face center must be maintained, and the face cell nodes will rotate around the face center. The corrected node values of the face cell can be calculated as follows:

$$P_{i,j} = OM_{i,j} \cdot (\sin\alpha - \cos\beta), \tag{22}$$

where $P_{i,j}$ is the corrected value of the vertices on face i, the subscript i represents the face series number and subscript j is the series number of a point on face i; $O_iP_{i,j}$ is the distance from the face center to the face vertices; $O_iM_{i,j}$ is the projection of $O_iP_{i,j}$ on the steepest slope direction; α is the angle between the bed face and the horizontal plane, and β is the sediment angle of repose.

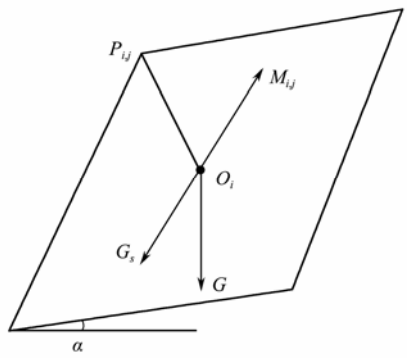

Fig.2 Schematic view of sand slide model.

3 Numerical Simulation Schemes

3.1 Numerical Flow Model Schemes

The governing equations of the CFD model are Navier-Stokes (N-S) equations, which we discretize using the finite volume method. Currently, one of the following three methods is usually adopted to solve for pressure-velocity coupling: the pressure-implicit splitting of operators (PISO), the semi-implicit method for pressure-linked equations (SIMPLE), and the PIMPLE coupling method which combines the PISO and SIMPLE. In our scour model, we use the PIMPLE scheme.

To solve for the bed boundary layer, the mesh grid near the bed must be equally fine as those in the common CFD codes since the boundary layer is usually quite thin. In our scour model, we used the wall function to resolve the boundary layer problem, which can save simulation time. We divide the computational zone into two parts: the boundary layer zone, which is resolved using empirical equations, and the turbulent layer zone, which is calculated using a turbulence closure model such as *k-ε, k-ω* or the large eddy simulation (LES) model. With this method, the first layer mesh grid need not be in the boundary layer.

3.2 Numerical Schemes for Sediment Transport and Scour Model

Bedload and suspended load are independent variables, and we solve for them, respectively, in the sediment transport model. We can determine the bed shear stress, Shields number, and the bed load transport rate after modeling the flow velocity. When simulating flow, we can directly calculate the bed load and we calculate the suspended load using the convection-diffusion equation, which yields the transport by the flow field. We use the finite volume method to solve this equation. We calculate the erosion rate using the empirical formula after the flow model computation is finished. We can determine the deposition rate of the suspended load after solving the convention-diffusion equation.

We solve the Exner equation to obtain the bed evolution based on the sediment transport parameters obtained in the previous calculations. The dimensions of the Exner equation are usually less than those of the flow model, so the sediment information must be mapped from 3D to 2D or from 2D to 1D. In this study, we use the FAM to solve this problem.

The time step of the flow simulation is small. If we solve for the morphology with this time step, it will take a great amount of computation time. To increase the modeling speed, we use the time marching scheme in which the time step of the morphology model is ten times that of the flow simulation.

The scour model procedure can be summarized as follows:

1) Solve the N-S equations to obtain the flow field information and calculate the bed shear stress, suspended sediment concentration, and bedload transport rate.

2) Compute the erosion rate and deposition rate of the suspended sediment and use FAM to solve the Exner equation to obtain the change in the bed elevation.

3) Solve the Laplacian equation to obtain the movement of the mesh vertices and then move mesh points using the assigned values.

4) Apply the sand slide model to adjust the bed when the bed angle is larger than the angle of repose.

5) Move the mesh points to the new locations, which have been corrected in step 4, until all the angles are smaller than the angle of repose.

6) Go to the next time step and repeat steps 1–5 until the specified time has been reached.

4 Model Validation

Next, we conducted three tests to validate the sand slide model and the suspended sediment and scour models, respectively. The first test is a constant slope case, which we used to test the sand slide model; the second is a net entrainment experiment, which we used to test the suspended sediment transport model; and the last is a wall jet scour test, which we used to validate the scour model.

4.1 Sand Slide Model Test

To validate the sand slide model, we used a constant slope of 45 degrees, assuming the sediment angle of repose to be 30 degrees. After the simulation, the constant

slope should be 30°. Fig.3 shows the slope changes after the effect of the sand slide model. After implementing this model, we found all the bed slope angles to be less than or equal to the angle of repose. This result shows that the sand slide model can work well when the bed slope angle exceeds the angle of repose.

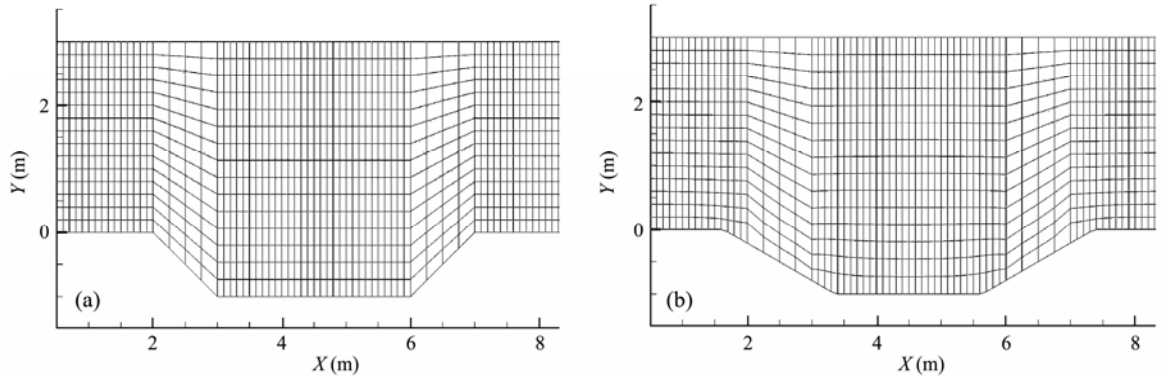

Fig.3 Waterway section before and after implementation of the sand slide model: a) before sand slide; b) after sand slide.

4.2 Suspended Load Entrainment Experiment

We validated the suspended load model in a van Rijn's net entrainment experiment, a schematic view of which is shown in. Fig.4. In the experiment, we divided the bed into loose and rigid sections, with the loose sand bed preceded by the rigid bed section. The sediments were entrained from the loose bed into suspension before the sediment concentration reached equilibrium. The water depth was 0.25 m and the inlet velocity was 0.67 m s^{-1}. The sand particle diameter was 0.2 mm and the corresponding setting velocity was 0.022 m s^{-1}.

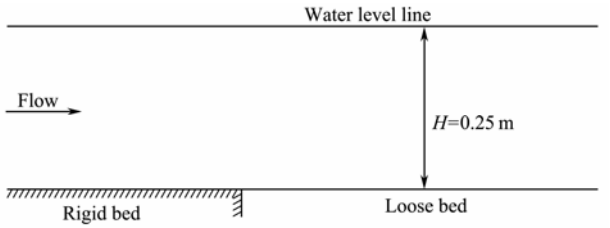

Fig.4 Schematic view of the entrainment experiment.

In this simulation, to more clearly demonstrate the suspended sediment module, we closed the scour and bedload models. We used the *k-ε* closure model to simulate the turbulence. For fully developed turbulence, we set the lengths of the rigid and loose beds as 20*H* and 60*H* (where *H* is depth), respectively. We set the suspended concentration of the inlet at zero for clear water. The suspended load was mainly entrained from the loose bed, so we assigned the sediment concentration in the loose bed boundary. We can compute the equilibrium concentration in the bed boundary using Eq. (19) or the method of Van Riji (1987). After computing the non-dimensional parameter, we multiplied it by the density of the sand to compute the bed concentration. In this model, the equilibrium concentration of the bed boundary is 3.9 kg m^{-3}. More details regarding the parameters can be found in the paper by Liang *et al.* (2005). We abstracted the concentration profiles at $x=4H$, $10H$, $20H$, and $40H$ to validate the simulation results, as shown in Fig.5. We can see from the figure that the sediment concentration profile is parabolic. From the bed to the water surface, the sediment concentration decreases rapidly. At a depth of 0.15 m above the bed, the concentration is very low, close to zero. The modeled result fits well with the experimental data. At the $x=40H$ location, the sediment concentration given by the numerical model is lower than the measured one, which might be due to the decay of flow velocity.

4.3 Wall Jet Scour Test

Chatterjee *et al.* (1980) conducted an experiment to investigate the effect of a submerged wall jet on the flow field and sediment transport. To validate the local scour model, we simulated this experiment using our developed model. Case Run2 of this experiment is a classical test, a schematic view of which is shown in Fig.6. As we can see in the figure, the jet width B_0 was 0.02 m and the apron length L_0 was 0.66 m. The inlet flow velocity was 1.56 m s^{-1}, which is controlled by the upstream and downstream water levels. The upstream water level was 0.409 m and that of the downstream was 0.291 m. The sand diameter was 0.76 mm and the porosity was 0.43. The angle of repose was 30° and the static friction coefficient was 0.63. The critical Shields number was 0.04. To simulate the turbulence, we used the renormalization group (RNG) *k-ε* model, which is a developed standard *k-ε* model. To simplify the simulation, we also simulated the downstream of the sluice gate.

Before the simulation, we performed a mesh convergence study in which we simulated four different mesh size cases of 1 cm, 5 mm, 1 mm, and 0.5 mm. We then abstracted the near-bottom velocity at $x=0.6$ m and $x=1.0$ m, and the results are shown in Table 1. We found the modeled results to more closely resemble the measured results when the mesh size was finer, but there was no significant improvement with mesh sizes finer than 1 mm. Thus, in this work, we adopted a mesh size of 1 mm in the next simulation.

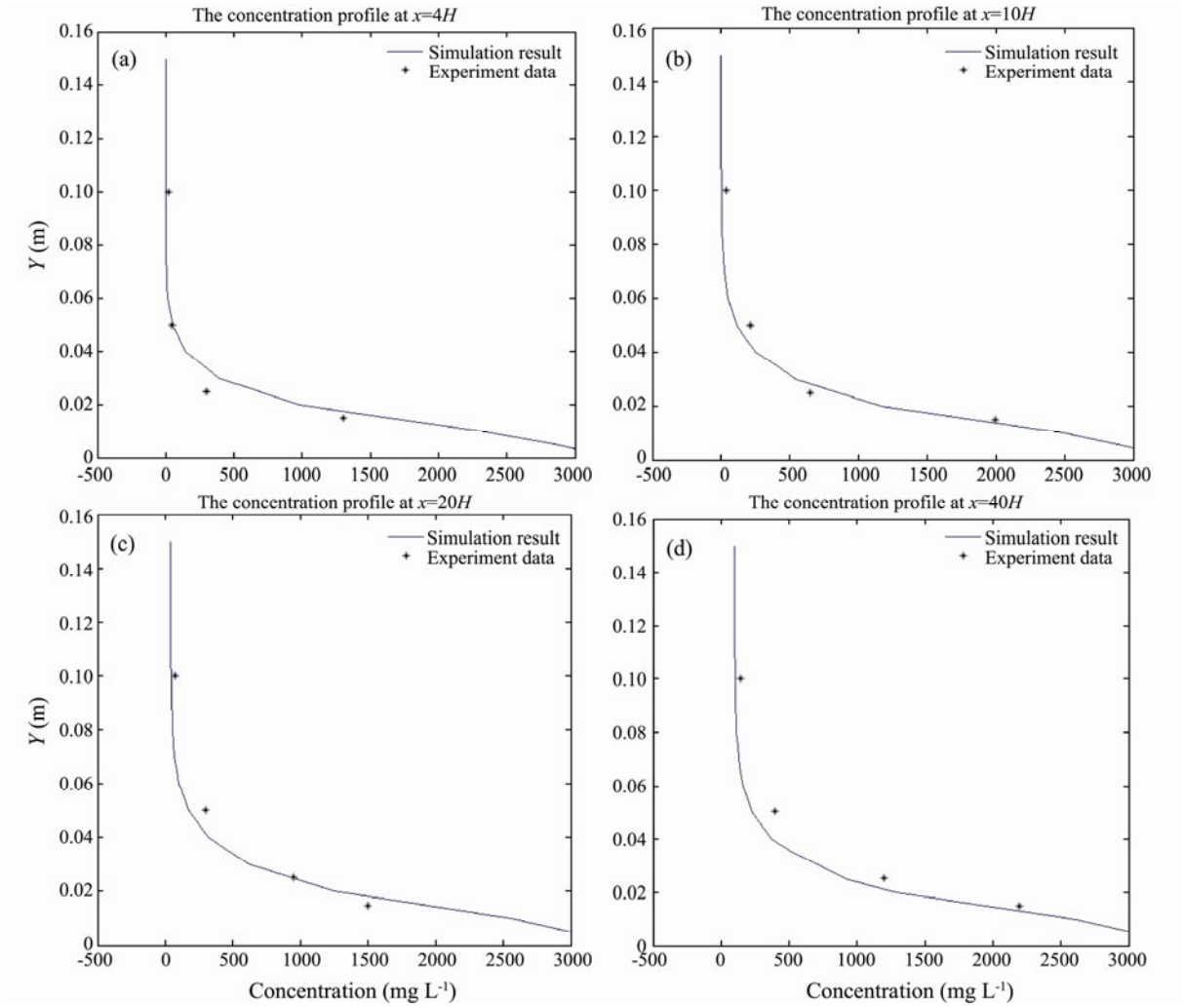

Fig.5 Sediment concentration profile at assigned locations.

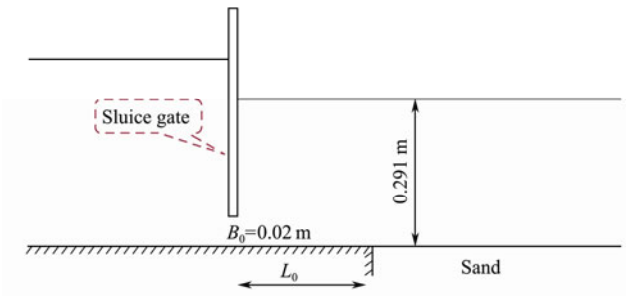

Fig.6 Schematic view of the wall jet scour experiment.

Table 1 Simulated bottom velocity response to the mesh size

Cases	Location	
	$x=0.6$ m	$x=1.0$ m
Experiment data	0.905	0.312
Case1 (mesh size 1 cm)	1.023	0.452
Case2 (mesh size 5 mm)	0.946	0.406
Case3 (mesh size 1 mm)	0.916	0.382
Case4 (mesh size 0.5 mm)	0.911	0.374

Flow velocity plays an important role in the development of scour depth and the accuracy of the flow has obvious effects on the precise development of scour. Fig.7 shows the modeled and measured turbulence wall jet characteristics and Fig.7(a) shows the jet diffusion along the x-axis. The x-axis is the logarithmic function of the non-dimensional distance x/B_0, where B_0 is the width of the jet. The y-axis is the logarithmic function of the non-dimensional velocity u/u_0, with u_0 being the inlet velocity 1.56 m s^{-1}. The experiment data was reproduced well by the numerical simulation. In the experiment, the diffusion process changed slowly on the apron, whereas in the bed erosion zone, the changes occurred quickly. The turbulence energy was underestimated by the numerical model. Fig.7(b) shows the distribution of the non-dimensional flow velocity at $x=0.6$ m. The x-axis represents the non-dimensional distance y/σ, where σ is the vertical distance from the wall to the location of the maximum horizontal velocity. The y-axis represents the non-dimensional flow velocity v/V_{max}, where V_{max} is the maximum horizontal velocity of section $x = 0.6$ m. From the bottom to the water level, the horizontal flow velocity increases fast and then decreases slowly, with the maximum horizontal velocity occurring 0.012 m above the bottom. In other words, the numerical model can calculate the velocity distribution well.

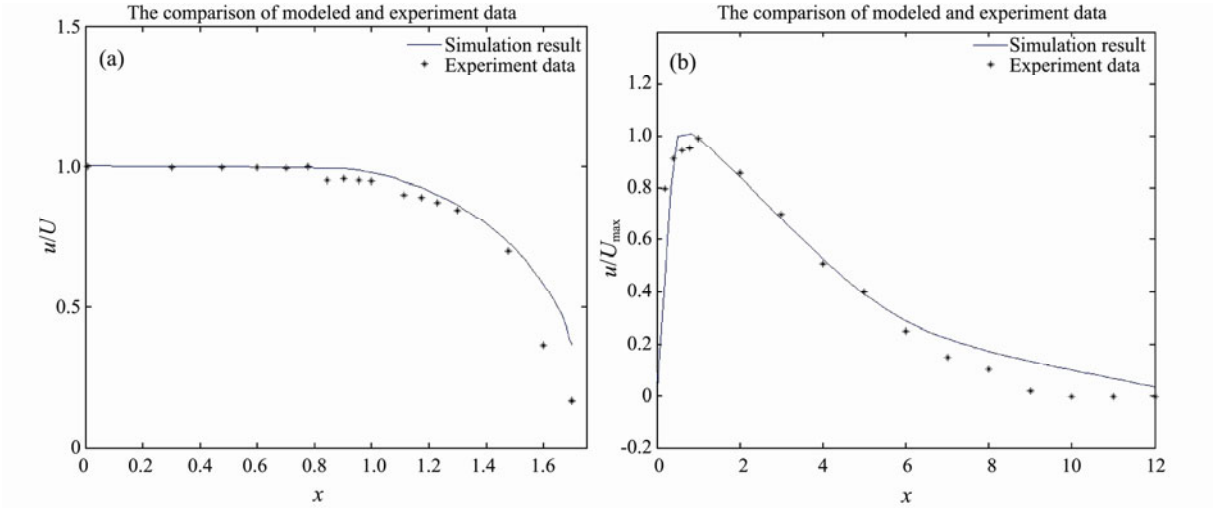

Fig.7 The turbulence wall jet characteristic.

To study the flow in a steady state, Fig.8 shows the velocity vector field at $t=20$ s, when no scour occurs. When the flow goes through the jet, a vortex appears at the back of the sluice gate due to the separation of the boundary layer. There are also some other small vortices in the back of the sluice gate zone. In the steady state, the water level changed from 0.291 m to 0.32 m, which is similar to the results reported by Liu (2008).

Fig.9 shows the development of the maximum scour depth and deposition height, in which the profile shows a logarithmic function distribution. Within the first 20 minutes, the maximum scour depth developed rapidly, and the scour development was up to about 90% of the maximum equilibrium scour depth. At 60 minutes, the scour hole reached equilibrium. The maximum scour depth was 0.072 m and the maximum deposition depth was 0.075 m. These equilibrium scour depth and deposition height values are somewhat overestimated, which might be mainly due to the overestimated flow velocity by the flow model.

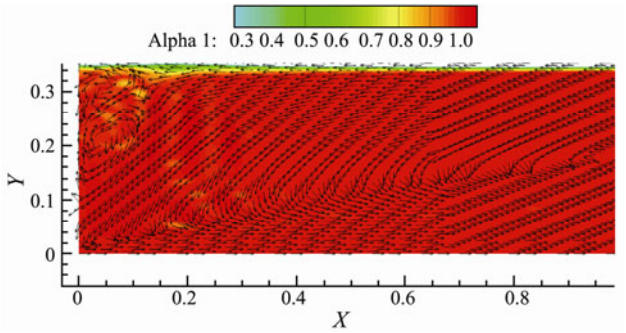

Fig.8 Velocity profile of steady state without scour.

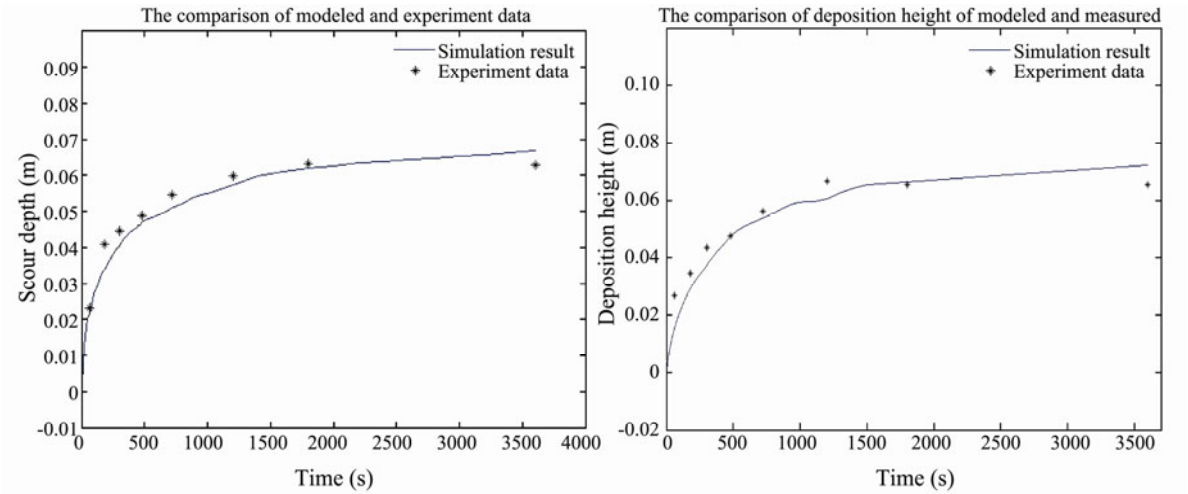

Fig.9 Maximum scour depth and deposition height with time.

Fig.10 shows plots of the scour profiles at different times, which are sinusoidal. The modeled scour profiles agree well with the measured ones. However, the errors for locations from $x=0.66$ m to $x=0.71$ m are greater those at other locations, which we can attribute to the common point shared by the bed and apron. Fig.11 shows the velocity vector field at $t=60$ min, in which we see that the vortex size has decreased and the water level around the scour hole has increased to higher than that of the apron zone.

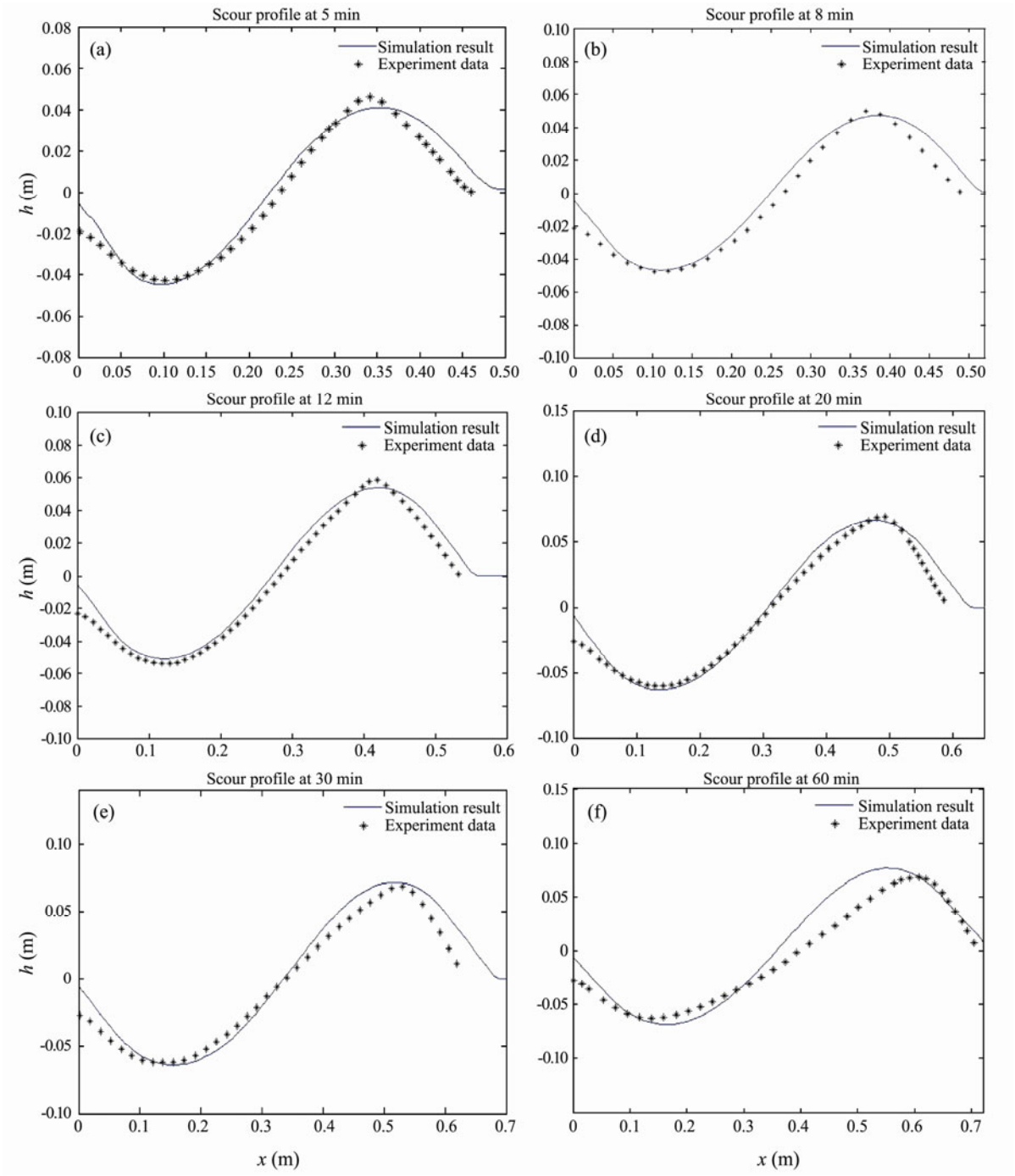

Fig.10 Scour profile at different times.

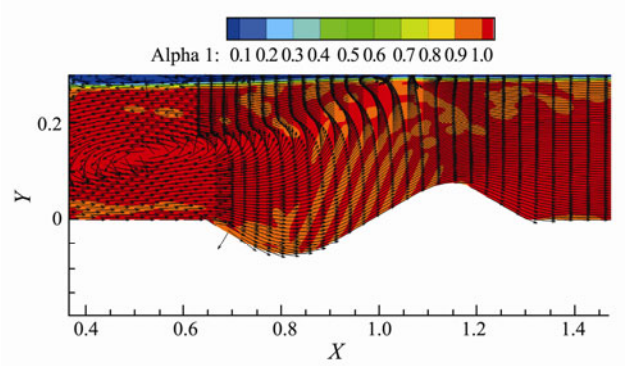

Fig.11 Velocity vector field at equilibrium state.

5 Conclusions

In this work, we developed a numerical scour model for calculating the scour process and the equilibrium scour around hydraulic structures. We set and combined the bedload and suspended load of the sediment transport model using the OpenFOAM source code and took into account the influences of the bed slope on the bedload. We constructed a sand slide method to smooth the bed surface when it exceeds the slope of the angle of repose and used a constant slope case in our demonstration. We proposed a time marching scheme to reduce computational time and introduced a dynamic mesh method to

model the evolution of the bed elevation. We conducted three typical experiments to validate our developed numerical model.

Using a 45-degree constant slope, we showed that the sand slide model works well when the bed slope angle exceeds the angle of repose. We validated the suspended load model using van Rijn's net entrainment experiment. The modeled results generally fit well with the experimental data and the scour profiles simulated by our developed model agree with those of the experiment conducted by Chatterjee *et al.* (1980).

All of the validation results confirm that the scour model, in general, can accurately simulate the scour process and equilibrium scour. As such, we can conclude that our numerical model is effective in simulating the scour processes that play an important role in hydraulic structure stability.

Acknowledgements

The authors would like to acknowledge the support from the State Key Laboratory of Hydraulic Engineering Simulation and Safety Foundation (No. HESS-1412), the National Science Fund (No. 51179178), and the 111 Project (No. B14028).

References

Baykal, C., 2014. Development of a numerical 2-dimensional beach evolution model. *Turkish Journal of Earth Sciences*, **23** (2): 215-231.

Bombar, G., Altinakar, M. S., Jia, Y. F., and Aksoy, A., 2013. 3D numerical simulation of local scouring around Bridge Piers under non-uniform sediment conditions. *Proceedings of 2013 IAHR World Congress.* Beijing, 120-131.

Chatterjee, S. S., Ghost, S. N., and Chatterjee, M., 1994. Local scour due to submerged horizontal jet. *Journal of the Hydraulic Engineering*, **120** (8): 973-992.

Fuhrman, D. R., Baykal, C., Sumer, B. M., Jacobsen, N. G., and Fredsøe, J., 2014. Numerical simulation of wave-induced scour and backfilling processes beneath submarine pipelines. *Coastal Engineering*, **94**: 10-22.

Huai, W. X., Wang, Z. W., Qian, Z. D., and Han, Y. Q., 2011. Numerical simulation of sandy bed erosion by 2D vertical jet. *Science China Technological Science*, **54** (12): 3265-3274.

Huang, W. R., Yang, Q. P., and Xiao, H., 2009. CFD modeling of scale effects on turbulence flow and scour around bridge piers. *Computers & Fluids*, **38**: 1050-1058.

Jacobsen, N. G., 2011. A full hydro- and morphodynamic description of breaker bar development. PhD thesis. Technical University of Denmark.

Jacobsen, N. G., 2015. Mass conservation in computational morphodynamics: Uniform sediment and infinite availability. *International Journal for Numerical Methods in Fluids*, **78** (4): 233-256.

Jasak, H., and Tuković, Z., 2007. Automatic mesh motion for the unstructured finite volume method. *Transactions of FEMENA*, **30** (6): 1-18.

Liang, D. F., Cheng, L., and Li, F. J., 2005. Numerical modeling of flow and scour below a pipeline in currents part II. Scour simulation. *Coastal Engineering*, **52** (1): 43-62.

Liu, X. F., 2008. Numerical models for scour and liquefaction around object under currents and waves. PhD thesis. University of Illinois at Urbana Champaign.

Niemann, S. L., Fredsøe, J., and Jacobesen, N. G., 2011. Sand dunes in steady flow at low Froude numbers: Dune height evolution and flow resustance. *Journal of Hydraulic Engineering*, **137**: 5-14.

Petersen, T. U., 2014. Scour around offshore wind turbine foundations. PhD thesis. Technical University of Denmark.

Roulund, A., Sumer, B. M., Fredsoe, J., and Michelsen, J., 2005. Numerical and experimental investigation of flow and scour around a circular pile. *Journal of Fluid Mechanics*, **534**: 351-401.

Roulund, A., Sumer, B. M., Fredsoe, J., and Michelsen, J., 2005. Numerical and experimental investigation of flow and scour around a circular pile. *Journal of Fluid Mechanics*, **534**: 351-401.

Stahlmanm, A., 2013. Numerical and experimental modeling of scour at foundation structures for offshore wind turbines. *Proceedings of the Twenty-Third International Offshore and Polar Engineering.* Alaska, USA, 131-138.

Sumer, B. M. Güner, A., Hansen, N. M., Fuhrman, D. R., and Fredsøe, J., 2011. Flow and sediment transport induced by plunging waves. *Journal of Geophysical Research Oceans*, **116**: 114-120.

Van Rijn, L. C., 1987. *Mathematical Modelling of Morphological Processes in the Case of Suspended Sediment Transport*. Delft Hydraulics Communication Press, Delft, Holland, 45pp.

Vasquez, J. A., and Walsh, B. W., 2009. CFD simulation of local scour in complex piers under tidal flow. *33rd IAHR congress: Water Engineering for a Sustainable Environment.* Vancouver, Canada, 913-920.

Zhao, M., Vaidya, S., Zhang, Q., and Cheng, L., 2015. Local scour around two pipelines in tandem in steady current. *Coastal Engineering*, **98**: 1-15.

(Edited by Xie Jun)